

Article

# Phenylspirodrimane with Moderate Reversal Effect of Multidrug Resistance Isolated from the Deep-Sea Fungus *Stachybotrys* sp. 3A00409

Xinhua Ma <sup>1</sup>, Min Wu <sup>1,2</sup>, Zhenwei Chen <sup>1</sup>, Fan Cao <sup>1</sup>, Tianhua Zhong <sup>3</sup>, Zhuhua Luo <sup>3</sup>, Zongze Shao <sup>3</sup>, Yonghong Zhang <sup>1</sup>, Limin Chen <sup>1,\*</sup> and Zhiqiang Zhang <sup>1,\*</sup>

<sup>1</sup> Fujian Provincial Key Laboratory of Pharmacology of Natural Medicine, School of Pharmacy, Fujian Medical University, Fuzhou 350122, China; maxinhua@fjmu.edu.cn (X.M.); wumin@fjmu.edu.cn (M.W.); chenyi1314170@163.com (Z.C.); caofan0101@163.com (F.C.); zhangyh@fjmu.edu.cn (Y.Z.)

<sup>2</sup> Fuzhou Second Hospital, Fuzhou 350122, China

<sup>3</sup> Key Laboratory of Marine Biogenetic Resources, Third Institute of Oceanography, Ministry of Natural Sources, Xiamen 361005, China; zhongtianhua@tio.org.cn (T.Z.); luozhuhua@tio.org.cn (Z.L.); shaozongze@tio.org.cn (Z.S.)

\* Correspondence: chenlm5696@163.com (L.C.); zzq@fjmu.edu.cn (Z.Z.)

**Abstract:** Two new phenylspirodrimanes, stachybotrins K and L (1 and 2), together with eight known analogues (3–10), were isolated from deep-sea-derived *Stachybotrys* sp. MCCC 3A00409. Their structures were determined by extensive NMR data and mass spectroscopic analysis. Absolute configurations of new compounds were determined through a comparison of their circular dichroism (CD) spectra with other reported compounds. The possible reversal effects of all compounds were assayed in the resistant cancer cell lines. Stachybotrysin B (8) can reverse multidrug resistance (MDR) in ABCB1-overexpression cells (KBv200, Hela/VCR) at the non-cytotoxic concentration. Doxorubicin accumulation assay and molecular-docking analysis reveal that the mechanism of its reversal MDR effect may be related to the increase in the intracellular concentration of substrate anti-cancer drugs.

**Keywords:** deep-sea fungus; *Stachybotrys*; phenylspirodrimanes; multidrug resistance (MDR); reversal MDR effects

**Citation:** Ma, X.; Wu, M.; Chen, Z.; Cao, F.; Zhong, T.; Luo, Z.; Shao, Z.; Zhang, Y.; Chen, L.; Zhang, Z. Phenylspirodrimane with Moderate Reversal Effect of Multidrug Resistance Isolated from the Deep-Sea Fungus *Stachybotrys* sp. 3A00409. *Molecules* **2024**, *29*, 1685. <https://doi.org/10.3390/molecules29071685>

Academic Editors: Ericsson Coy-Barrera and Josphat Matasyoh

Received: 4 March 2024

Revised: 27 March 2024

Accepted: 5 April 2024

Published: 8 April 2024



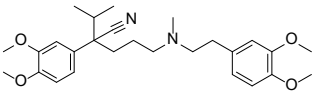
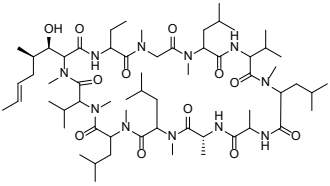
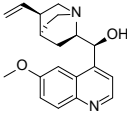
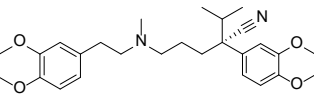
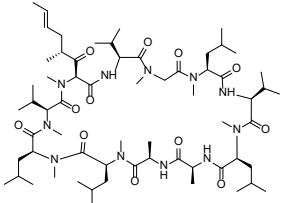
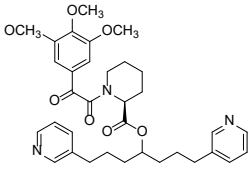
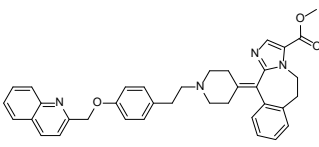
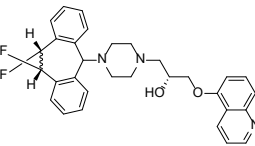
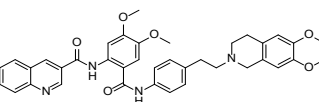
**Copyright:** © 2024 by the authors. Licensee MDPI, Basel, Switzerland. This article is an open access article distributed under the terms and conditions of the Creative Commons Attribution (CC BY) license (<https://creativecommons.org/licenses/by/4.0/>).

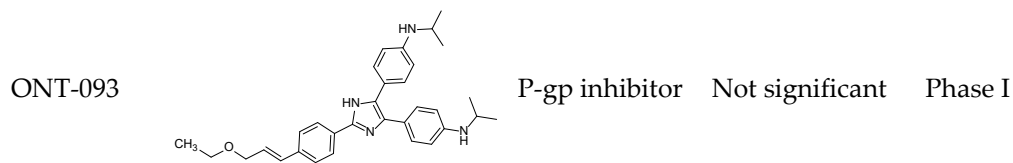
## 1. Introduction

Chemotherapy is the main treatment method for many malignant tumors. However, drug resistance is becoming a major problem in several cancers. Multidrug resistance (MDR) refers to the resistance of tumor cells to multiple chemotherapy agents, mediated by drug inactivation or the removal of drugs from target tumor cells [1,2]. MDR is currently considered to be one of the most common causes of cancer chemotherapy failure [3]. The most common mechanism of MDR is the overexpression of ABC transporters, which actively pump out large amounts of chemotherapy drugs from cancer cells, thereby weakening the efficacy of chemotherapy drugs [4,5]. The subfamily ABCB1/MDR1/P-glycoprotein, ABCC1/MRP1, and ABCG2/BCRP are the most extensively studied and considered as prime factors for the induction of MDR in tumor cells [6,7]. Among them, ABCB1/P-glycoprotein (P-gp) remains the best-studied and most potent ABC transporter to induce chemoresistance, and the upregulation of ABCB1/P-gp is closely linked with the emergence of MDR in tumor cells [8,9]. The discovery of ABCB1/P-gp suggests that combining ABCB1/P-gp inhibitors with traditional anticancer drugs may be a promising strategy for surmounting P-gp-mediated MDR [10,11]. In recent decades, three generations of ABCB1/P-gp inhibitors have been developed, some of which are currently undergoing

clinical trials to evaluate their role in circumventing anti-cancer resistance [9,12–16] (see Table 1). However, due to their unacceptable toxicity and problematic pharmacokinetic interactions, many of these inhibitors have not been used in clinical practice [8,17,18]. Therefore, there is still a strong demand for the screening of multidrug-resistance reversal agents and the development of new multidrug-resistance antagonists.

**Table 1.** Summary of major ABCB1/P-gp inhibitors in clinical development.

Name	Chemical Structure	Mechanism of Action	Adverse Effects	Phase
<b>First generation</b>				
Verapamil		Calcium channel blocker	Hypotension, cardiotoxicity	Phase II
Cyclosporine A		P-gp inhibitor	Not significant	Phase II
Quinine		P-gp inhibitor	Myelosuppression	Phase III
<b>Second generation</b>				
Dexverapamil		Calcium channel blocker	Cardiotoxicity	Phase II
Valspodar (PSC833)		P-gp inhibitor	Not significant	Phase III
Biricodar (VX-710)		P-gp inhibitor	Neutropenia	Phase II
<b>Third generation</b>				
Laniquidar (R101933)		P-gp inhibitor	Mucositis and neutropenic fever	Phase II
Zosuquidar (LY335979)		P-gp inhibitor	Neurotoxicity	Phase III
Tariquidar (XR9576)		P-gp inhibitor	Not significant	Phase II



Stachybotrys, a genus of filamentous fungi, is known to produce a broad range of secondary metabolites, such as macrocyclic trichothecenes, atranones, and phenylspirodrimanes (PSDs) [19,20]. PSDs belong to a type of meroterpenoids, which are proposed to be derived from the hybrid polyketide–terpenoid biosynthetic pathway. They feature a common drimane-type sesquiterpene skeleton connected with a benzene ring through a spirofuran ring and show high structural diversity [19]. To date, over 120 compounds of this class, including monomeric and dimeric PSDs, have been discovered to derive from *Stachybotrys* [19–23]. These metabolites are designated as the most dominant group of mycotoxins in this genus [19,20,24]. PSDs can be further divided into three main classes: tetracyclic aromatic sesquiterpenoids with alcohol and/or aldehyde side chains, like stachybotrydial, pentacyclic aromatic sesquiterpenoids, such as stachybotrylactams and stachybotrylactones, and stachyflins with pentacyclic moiety including a *cis*-fused decalin [22,25]. They display diverse biological activities, including anticomplement, antiviral (HIV-1 and IAV) and anti-inflammatory activity, cytotoxicity, neuroprotective effects, tyrosine kinase inhibition, and tumor-related kinases inhibition [19]. Active monomeric compounds are mostly concentrated in the first class with alcohol and/or aldehyde functionalities and stachybotrylactones [19].

In our prior work, a series of phenylspirodrimanes were isolated from a deep-sea-derived *Stachybotrys* sp. MCCC 3A00409 [26]. Attracted by their interesting structures, subsequent chemical investigation led to the isolation of two new phenylspirodrimanes (1–2), together with eight known derivatives (3–10), which were identified as stachybonoid E (3) [27], stachybotrin H (4) [26], stachybotrin E (5) [28], stachybotrylactam acetate (6) [29],  $\alpha$ -acetoxystachybotrylactam acetate (7) [29], stachybotrysin B (8) [30], stachybotrysin H (9) [26], and Mer-NE5003E (10) [31] from the oats solid culture (Figure 1). In our research, we discovered that stachybotrysin B (8) had a reversal effect on MDR in ABCB1-overexpressing cancer cells. This paper described the isolation, structure elucidation, and bioactivity of these compounds.

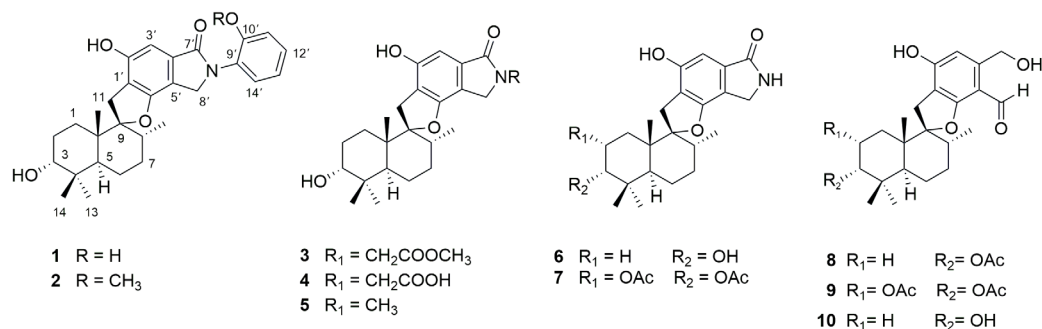


Figure 1. Chemical structures of compounds 1–10.

## 2. Results and Discussion

### 2.1. Structural Determination

*Stachybotrys* sp. MCCC 3A00409 was cultured on solid oats and rice medium for 30 days at 28 °C. The organic extract prepared by solvent extraction was fractionated by repeated silica gel column chromatography (CC), ODS CC, Sephadex LH-20 CC, and, finally, semi-preparative HPLC to yield compounds **1–10** (Figure 1).

Stachybotrin K (**1**) was obtained as a pale yellow oil. The HRESIMS peaks at  $m/z$  478.2593  $[M + H]^+$  suggested the molecular formula of  $C_{29}H_{35}NO_5$ , requiring thirteen degrees of unsaturation. A comparison of the 1D NMR data (Table 2) with those of the known compound **5** (stachybotrin E) [28] revealed that they shared the same phenylspirodrimane skeleton, except for the replacement of N-CH<sub>3</sub> in **5** by an ortho-substituted phenol group in **1**. The phenol unit was determined by the COSY correlations of H-11'/H-12'/H-13'/H-14' and the HMBC correlations from H-11' ( $\delta_H$  6.96, d,  $J = 8.0$  Hz) to C-9' ( $\delta_C$  125.7), C-10' ( $\delta_C$  152.8), and C-13' ( $\delta_C$  119.2), and from H-14' ( $\delta_H$  7.31, d,  $J = 6.9$  Hz) to C-9', C-10', C-12' ( $\delta_C$  128.2) (Figure 2). Although the HMBC spectrum did not give the correlations from H-14' to C-8', the NOESY cross-peaks between H-14' ( $\delta_H$  7.31) and H-8' ( $\delta_H$  4.62), as shown in Figure 2, suggested that the phenol moiety was connected to the nitrogen atom. The planar structure of **1** was further confirmed by 2D NMR data (Figure 2). NOESY correlations H-3/Me-14, Me-14/Me-15, Me-15/H-8, Me-15/H<sub>2</sub>-11, and OH-3/Me-13, Me-13/H-5, H-5/H $\alpha$ -7, H $\alpha$ -7/Me-12 determined that H-3, Me-14, and Me-15 are in  $\beta$ -orientations, while Me-13, H-5, and Me-12 are in  $\alpha$ -orientations (Figure 2). The absolute configuration of **1** was assigned to be 3*R*, 5*S*, 8*R*, 9*R*, and 10*S* on the basis of its ECD spectrum, which exhibited similar Cotton effects (CEs) (negative CEs were observed at 245 and 266 nm, while positive CEs were observed at 310 nm) (Figure 3) to those of stachybotrin E (**5**) [28].

**Table 2.** 1D NMR data (400/100 MHz, DMSO-*d*<sub>6</sub>) for compounds **1** and **2**.

No.	<b>1</b>		<b>2</b>	
	$\delta_C$	$\delta_H$ (J in Hz)	$\delta_C$	$\delta_H$ (J in Hz)
1	23.9, CH <sub>2</sub>	0.94, m; 1.79, m	23.9, CH <sub>2</sub>	0.94, m; 1.78, m
2	24.9, CH <sub>2</sub>	1.37, m; 1.76, m	24.9, CH <sub>2</sub>	1.36, m; 1.75, m
3	73.5, CH	3.17, brs	73.5, CH	3.16, brs
4	36.5, C		36.5, C	
5	39.9, CH	2.01, d (8.3)	39.9, CH	2.00, m
6	20.5, CH <sub>2</sub>	1.42, m; 1.46, m	20.5, CH <sub>2</sub>	1.41, m; 1.45, m
7	30.8, CH <sub>2</sub>	1.39, m; 1.52, m	30.8, CH <sub>2</sub>	1.39, m; 1.51, m
8	37.3, CH	1.82, m	37.3, CH	1.81, m
9	98.1, C		98.1, C	
10	41.8, C		41.9, C	
11	31.7, CH <sub>2</sub>	3.14, d (17.5) 2.79 (d, 17.0)	31.7, CH <sub>2</sub>	3.14, d (17.9) 2.79, d (17.1)
12	15.6, CH <sub>3</sub>	0.68, d (6.4)	15.6, CH <sub>3</sub>	0.68, d (6.4)
13	28.7, CH <sub>3</sub>	0.86, s	28.7, CH <sub>3</sub>	0.86, s
14	22.4, CH <sub>3</sub>	0.79, s	22.4, CH <sub>3</sub>	0.79, s
15	15.8, CH <sub>3</sub>	0.95, s	15.8, CH <sub>3</sub>	0.95, s
1'	117.1, C		117.2 s	
2'	153.8, C		153.9 s	
3'	101.1, CH	6.64, s	101.2, CH	6.64, s
4'	133.6, C		133.5, C	
5'	112.5, C		112.4, C	
6'	155.9, C		155.9, C	
7'	167.2, C		167.1, C	

8'	48.8, CH <sub>2</sub>	4.62, brs	49.0, CH <sub>2</sub>	4.53, dd (16.2) 4.61, dd (16.2)
9'	125.7, C		126.8, C	
10'	152.8, C		154.9, C	
11'	116.8, CH	6.96, d (8.0)	112.4, CH	7.15, d (8.2)
12'	128.2, CH	7.17, t (7.6)	128.7, CH	7.34, t (7.8)
13'	119.2, CH	6.86, t (7.5)	120.5, CH	7.01, t (7.6)
14'	128.6, CH	7.31, d (6.9)	129.0, CH	7.36, dd (7.6, 1.6)
15'			55.6, CH <sub>3</sub>	3.79 s
3-OH		4.09, d (2.9)		4.11, d (2.6)

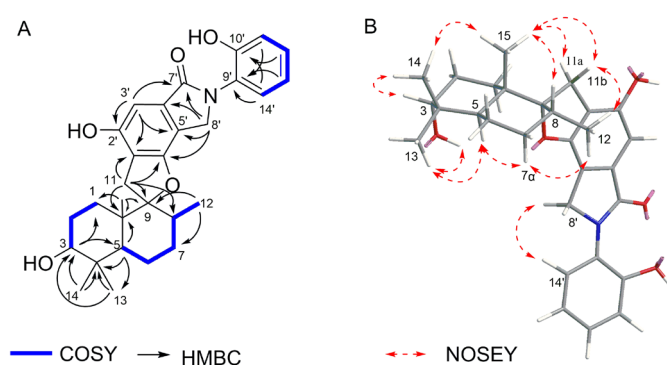


**Figure 2.** Key <sup>1</sup>H-<sup>1</sup>H COSY, HMBC correlations (A) and NOESY correlations (B) of compound 1.

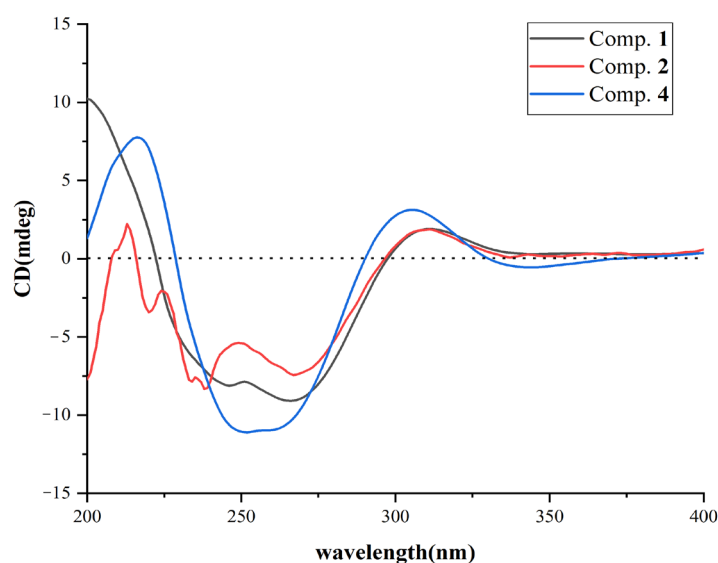


**Figure 3.** ECD spectra of compounds 1, 2, 4.

Compound 2 was obtained as a pale yellow oil and was assigned the molecular formula of C<sub>30</sub>H<sub>37</sub>NO<sub>5</sub> on the basis of HRESIMS at *m/z* 514.2570 [M + Na]<sup>+</sup> (calcd. For 514.2569), along with <sup>1</sup>H and <sup>13</sup>C NMR spectroscopic data (Table 2). The structure of 2 was determined as a methylated analogue of 1 on the basis of the close similarity of NMR data, except for the presence of the methoxyl resonances at  $\delta_{\text{H}}$  3.79 (3H, s) and  $\delta_{\text{C}}$  55.6, while the methoxy group was substituted at OH-10', as evident from the correlation between H<sub>3</sub>-15' ( $\delta_{\text{H}}$  3.79) and C-10' ( $\delta_{\text{C}}$  154.9) (Supplementary Materials: Figure S1). The relative configuration of the phenylspirodrimane moiety in 2 was further established by its NOESY correlations (Figure S1). According to the similar chemical shifts from 2 to 1 (Figure 3) and

the associated Cotton effects (CEs), the absolute configuration of compound **2** was identified as being as same as **1**. Therefore, the structure of compound **2** was determined and given the name of stachybotrin L. When compound **1** was stirred with silica in MeOH for 48 h, compound **2** was not detected by HPLC-UV analysis. Therefore, we confirmed that compound **2** was not an artifact product.

Stachybotrin H (**4**) was previously isolated from the same strain [26], but the absolute configuration was not established. Through a comparison of its ECD curves with **1** and **2** (Figure 3), the absolute configuration of **4** was also established as 3*R*, 5*S*, 8*R*, 9*R*, and 10*S*.

## 2.2. Biological Assays

To quickly screen for compounds with resistance reversal activity, we used flow cytometry analysis to detect the effects of compounds **1–10** on the accumulation of doxorubicin (DOX) in the resistant human oral epithelial cancer cell line KBv200. The results showed that compound **8** could increase the accumulation of DOX in KBv200 cells at 20  $\mu$ M (Figure 4).

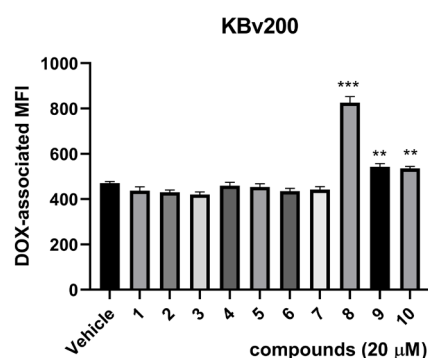


**Figure 4.** The effect of compounds **1–10** on the accumulation of DOX in KBv200 cells. \*\*  $p < 0.01$ , \*\*\*  $p < 0.001$  versus control group.

To find the suitable concentrations of compound **8** for reversing MDR in vitro, we first examined the cytotoxic effect of **8** on different cancer cell lines via MTT assay. As shown in Figure 5, stachybotrysin B (**8**) had almost no significant cytotoxic effect on KB, KBv200 cells at concentrations below 10  $\mu$ M, and had no cytotoxic effects on HeLa and HeLa/VCR below 80  $\mu$ M, after 72 h of treatment. In addition, compound **8** showed no cytotoxic activity against normal H9C2 cells below 40  $\mu$ M (Figure 5E). Thus, we chose concentrations of 10  $\mu$ M and 20  $\mu$ M as the maximum concentrations for further reversal assays in KBv200 and HeLa/VCR cell lines, respectively; at the chosen concentrations, more than 90% of cells survived.

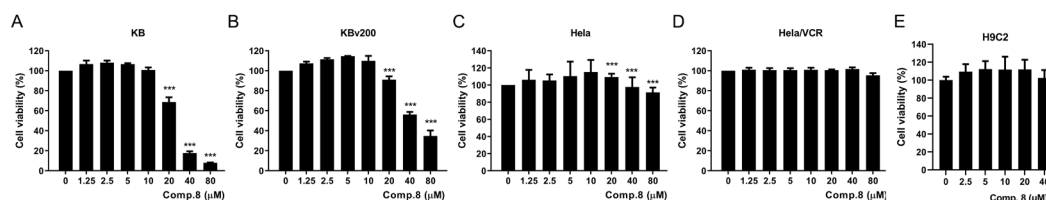


**Figure 5.** Cytotoxicity of compound **8** (comp. **8**) in pairs of cancer cells or normal cells. (A) ABCB1-negative KB cells; (B) ABCB1-overexpressing KBv200 cells; (C) ABCB1-negative HeLa cells; (D) ABCB1-overexpressing HeLa/VCR cells; (E) rat cardiomyocytes H9C2 cells. \*\*\*  $p < 0.001$  versus control group.

Then, we investigated the reversal effect of compound **8** on different tumor-sensitive cell lines and their drug-resistant cell lines. The results (Table 3) revealed that compound **8** exhibited moderate resistance reversal effects against the substrate chemotherapeutic agents, DOX and navelbine (NVB), in the ABCB1-overexpressing drug-resistant cell line KBv200, and against DOX in the ABCB1-overexpressing drug-resistant cell line HeLa/VCR, with fold resistance ranging from 1.54 to 4.86 and from 1.43 to 7.82, respectively, in a dose-dependent manner. However, compound **8** did not significantly decrease the IC<sub>50</sub> of cisplatin, which was not a substrate chemotherapeutic drug of ABCB1, in the ABCB1-overexpressing MDR cells. These results indicated that compound **8** could reverse ABCB1-mediated MDR.

**Table 3.** MDR-reversal effects of compound **8** on ABCB1 substrate drugs and non-substrate drugs.

Compound	IC <sub>50</sub> ± SD μM (Fold Reversal)			
	KB		KBv200	
Doxorubicin	0.007 ± 0.008		3.706 ± 1.224	
+5 μmol L <sup>-1</sup> <b>8</b>	0.007 ± 0.007	1.00	2.414 ± 1.814	1.54
+10 μmol L <sup>-1</sup> <b>8</b>	0.007 ± 0.007	1.00	1.897 ± 1.648	1.95
Navelbine	0.001 ± 0.0001		2.514 ± 2.271	
+5 μmol L <sup>-1</sup> <b>8</b>	0.001 ± 0.0001	1.00	0.800 ± 0.240	3.14
+10 μmol L <sup>-1</sup> <b>8</b>	0.001 ± 0.0001	1.00	0.517 ± 0.007	4.86
Cisplatin	0.385 ± 0.204		0.810 ± 0.377	
+5 μmol L <sup>-1</sup> <b>8</b>	0.455 ± 0.234	0.84	0.913 ± 0.426	0.89
+10 μmol L <sup>-1</sup> <b>8</b>	0.493 ± 0.228	0.77	1.081 ± 0.482	0.75
	HeLa		HeLa/VCR	
Doxorubicin	0.098 ± 0.039		0.789 ± 0.575	
+5 μmol L <sup>-1</sup> <b>8</b>	0.074 ± 0.029	1.32	0.553 ± 0.410	1.43
+10 μmol L <sup>-1</sup> <b>8</b>	0.066 ± 0.018	1.48	0.324 ± 0.364	2.44
+20 μmol L <sup>-1</sup> <b>8</b>	0.083 ± 0.010	1.18	0.101 ± 0.045	7.82
Cisplatin	1.812 ± 1.075		0.873 ± 0.047	
+5 μmol L <sup>-1</sup> <b>8</b>	1.472 ± 0.861	1.23	0.954 ± 0.081	0.92
+10 μmol L <sup>-1</sup> <b>8</b>	1.749 ± 0.956	1.04	1.032 ± 0.032	0.85
+20 μmol L <sup>-1</sup> <b>8</b>	2.227 ± 1.289	0.81	1.363 ± 0.348	0.64

We further detected an effect of compound **8** on the intracellular accumulation of DOX, the substrate agents of the ABCB1 transporter, in ABCB1-overexpressing cell lines (KBv200, HeLa/VCR) via flow cytometry analysis. The results showed that compound **8** could increase the accumulation of DOX in KBv200 and HeLa/VCR, thereby increasing the concentration of DOX in these cancer cell lines at concentrations below 10 μM and 20 μM, respectively (Figure 6).

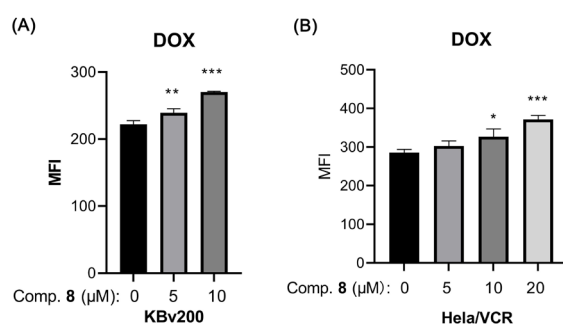


**Figure 6.** Effect of compound **8** on the accumulation of doxorubicin (DOX) in ABCB1-overexpressing KBv200 (A) and HeLa/VCR (B) cells. The results are presented as the mean fluorescence intensity (MFI) in ABCB1-overexpressing cells. \*  $p < 0.05$ , \*\*  $p < 0.01$ , \*\*\*  $p < 0.001$  versus the control group.

### 2.3. Docking Analysis of Compound 8 and Verapamil with ABCB1

Molecule docking simulation technology is a convenient and effective method to explore the interaction between small molecules and targets [32–35]. We performed a molecular docking simulation to characterize the molecular basis of the interactions between compound 8 and the human homology model of the ABCB1 transporter protein structure (PDB ID: 6QEX). The results (Figure 7) revealed that 8 was well-fitted at the substrate-binding site in the transmembrane domains (TMDs), with the highest docking score of  $-7.4$  kcal/mol. Then, we chose this protocol to dock verapamil (a classical ABCB1/P-gp inhibitor) [9] to TMDs. The docking score was  $-7.7$  kcal/mol.

For verapamil, a hydrogen bond is formed between the hydroxy group and GLN725 of ABCB1, and hydrophobic interactions are formed between verapamil and five amino acids, like ILE-340, PHE-983, PHE-336, ALA-229, and PHE-343 (Figure 7B). Similar to verapamil, compound 8 also interact with Gln725 of ABCB1 through H-bonds (Figure 7A). In addition, a hydrogen bond was found between the hydroxyl and aldehyde groups at the aromatic ring of and ALA-987 and ASN-721. The molecule was also predicted to interact with PHE-983, ALA-987, VAL-991, and PHE-336 via hydrophobic interaction. Thus, we can infer that the ABCB1 protein might recognize both 8 and verapamil through a similar mechanism.

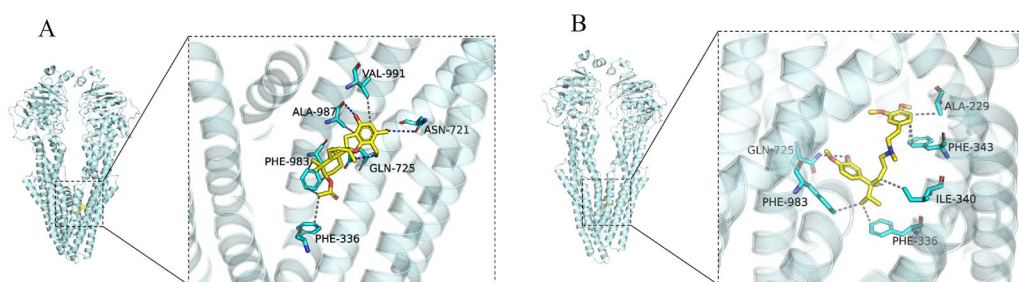


**Figure 7.** Docking of compound 8 (A) and verapamil (B) in the drug-binding pocket of ABCB1. Compound 8 and verapamil are shown as molecular models via yellow sticks. The light cyan cartoon represents ABCB1. Blue dashed lines represent hydrogen bonding, and gray dashed lines represent hydrophobic interactions.

## 3. Materials and Methods

### 3.1. General Experimental Procedure

Optical rotations were performed using a JASCO P-1020 digital polarimeter (Jasco Corporation, Tokyo, Japan). ECD spectra were obtained with a JASCO J-815 spectropolarimeter (Jasco Corporation, Tokyo, Japan). UV spectra were obtained using a Shimadzu UV-210A spectrometer (Shimadzu Corporation, Tokyo, Japan). NMR spectra were recorded with 400 and 600 MHz Bruker Avance NMR spectrometers (Bruker BioSpin AG, Fällanden, Switzerland). ESIMS was performed using a Shimadzu LCMS-8040 Liquid Chromatograph Mass Spectrometer (Shimadzu Corporation, Tokyo, Japan). HRESIMS spectra were obtained using a Thermo Scientific Ultimate 3000 UHPLC-Q Exactive spectrometer (ThermoFisher Scientific, Waltham, MA, USA). Semi-preparative HPLC was performed on a Waters 1525 system using a semi-preparative C18 (Waters SunFire C18 ODB Prep Column,  $10 \times 250$  mm,  $5 \mu\text{m}$ , 3 mL/min) column coupled with a Waters 2996 photodiode array detector (Waters Corporation, Milford, MA, USA). Thin-layer chromatography (TLC) was performed on plates precoated with silica gel GF254 ( $10\text{--}40 \mu\text{m}$ ) (Qingdao Marine Chemical Factory, Qingdao, China). Sephadex LH-20 (Amersham Biosciences, Uppsala, Sweden) and silica gel (100–200 and 200–300 mesh, Qingdao Marine Chemical Factory) were used for column chromatography.



### 3.2. Fungal Material

The fungus strain *Stachybotrys* sp. MCCC 3A00409 was isolated from Atlantic Ocean (−2807 m), as described previously [26]. The strain was deposited in the Marine Culture Collection Center (MCCC), Third Institute of Oceanography, Ministry of Natural Sources, and School of Pharmacy, Fujian Medical University.

The fungal strain was inoculated in the liquid medium (2.0% mannitol, 2.0% maltose, 1.0% glucose, 1.0% monosodium glutamate, 0.05%  $\text{KH}_2\text{PO}_4$ , 0.03%  $\text{MgSO}_4 \cdot 7\text{H}_2\text{O}$ , 0.3% yeast extract, 0.1% corn steep liquor, and 3.0% sea salt) in 500 mL shake flask with a loading of 150 mL as seed culture and incubated on a rotary shaker (165 rpm) at 28 °C for 2 days. A massive fermentation occurred in the solid medium (70 g oats, 20 g rice, distilled  $\text{H}_2\text{O}$  150 mL) using 300 mL × 60 Erlenmeyer flasks (1 L) and shaker fermentation at 28 °C for 35 days.

### 3.3. Extraction and Isolation

After incubation, the solid culture was extracted with  $\text{CH}_3\text{OH}$  three times. The  $\text{CH}_3\text{OH}$  extract was evaporated under reduced pressure to obtain an aqueous solution, and then the aqueous solution was extracted three times with EtOAc to obtain a brown crude gum (30.2 g).

The crude EtOAc extract was applied to a silica gel (200–300 mesh) column (180 g, 6.0 × 16.5 cm) and was separated into six fractions (Frs.1–6) using a step gradient elution of petroleum ether/ $\text{CH}_2\text{Cl}_2$  and  $\text{CH}_2\text{Cl}_2/\text{CH}_3\text{OH}$ . Fr.3 (3.6 g) was separated on a C-18 ODS column with a  $\text{CH}_3\text{OH}$ - $\text{H}_2\text{O}$  gradient (5–100%), producing six subfractions (Fr.3.1–Fr.3.6). Fr.3.3 was separated by Sephadex LH-20 using  $\text{CH}_3\text{OH}$  as the eluting solvent, and then on a semi-preparative HPLC column (75%  $\text{CH}_3\text{OH}/\text{H}_2\text{O}$ , 3.0 mL/min) to afford compounds **6** (20 mg,  $t_R$  = 32 min), **5** (5 mg,  $t_R$  = 35 min), and **7** (14 mg,  $t_R$  = 43 min). Fr.4 (5.1 g) was separated on a C-18 ODS column using step-gradient elution with  $\text{CH}_3\text{OH}/\text{H}_2\text{O}$  (5–100%) to obtain six subfractions (Fr.4.1–Fr.4.6). Subfraction Fr.4.3 was separated into seven subfractions (Fr.4.3.1–Fr.4.3.7) by Sephadex LH-20 eluted with  $\text{CH}_3\text{OH}$ . Fr.4.3.3 was purified by semi-preparative HPLC (75%  $\text{CH}_3\text{OH}/\text{H}_2\text{O}$ , 3.0 mL/min) to obtain compounds **3** (12 mg,  $t_R$  = 26 min) and **4** (8 mg,  $t_R$  = 31 min). Fr.4.3.4 was purified by semi-preparative HPLC (75%  $\text{CH}_3\text{OH}/\text{H}_2\text{O}$ , 3.0 mL/min) to obtain compounds **10** (7 mg,  $t_R$  = 30 min), **8** (20 mg,  $t_R$  = 34 min), and **9** (11 mg,  $t_R$  = 40 min). Fr.5 (2.4 g) was fractionated by Sephadex LH-20 eluted with  $\text{CH}_3\text{OH}$  and was further subjected, via semi-preparative HPLC (55%  $\text{CH}_3\text{CN}/\text{H}_2\text{O}$ , 3.0 mL/min) to obtain compounds **1** (6 mg,  $t_R$  = 36 min) and **2** (5 mg,  $t_R$  = 40 min).

Stachybotrin K (**1**): pale yellow oil;  $[\alpha]^{24\text{D}} -35.4$  ( $c$  0.10, MeOH); UV (MeOH)  $\lambda_{\text{max}}$  (log  $\epsilon$ ) 217 (3.93), 264 (3.05), 305 (2.55) nm; ECD ( $1.45 \times 10^{-4}$  M, MeOH)  $\lambda_{\text{max}}$  ( $\Delta\epsilon$ ): 200 (+10.24), 246 (−8.12), 266 (−9.08), and 311 (+1.90) nm;  $^1\text{H}$  and  $^{13}\text{C}$  NMR data shown in Table 1; HRESIMS:  $[\text{M} + \text{H}]^+ m/z$  478.2593 (calcd. for  $\text{C}_{29}\text{H}_{36}\text{NO}_5$ , 478.2593).

Stachybotrin L (**2**): pale yellow oil;  $[\alpha]^{24\text{D}} -38.2$  ( $c$  0.10, MeOH); UV (MeOH)  $\lambda_{\text{max}}$  (log  $\epsilon$ ) 216 (4.02), 263 (3.16), 303 (2.68) nm; ECD ( $1.05 \times 10^{-4}$  M, MeOH)  $\lambda_{\text{max}}$  ( $\Delta\epsilon$ ): 213 (+2.22), 238 (−8.32), 267 (−7.43), and 311 (+1.87) nm;  $^1\text{H}$  and  $^{13}\text{C}$  NMR data shown in Table 1; HRESIMS:  $[\text{M} + \text{Na}]^+ m/z$  514.2570 (calcd. for  $\text{C}_{30}\text{H}_{37}\text{NO}_5\text{Na}$ , 514.2569).

Stachybotrin H (**4**): colorless oil; ECD ( $1.33 \times 10^{-4}$  M, MeOH)  $\lambda_{\text{max}}$  ( $\Delta\epsilon$ ): 216 (+7.76), 252 (−11.10), 305 (+3.12), and 344 (−0.55) nm.

### 3.4. Cells and Materials

KB (human oral epidermoid carcinoma cell line) and its vincristine-selected ABCB1-overexpressing cell line KBv200, HeLa (human cervical carcinoma cell line) and its vincristine-selected ABCB1-overexpressing cell line HeLa/VCR, and rat cardiomyocytes cells H9C2 were cultured in RPMI 1640 medium supplemented with 10% FBS in the presence of 5% CO<sub>2</sub> at 37 °C. The commercial cell lines shown above were originally obtained from American-type culture collection (ATCC). All cells were grown in drug-free culture medium for more than 2 weeks before assay. Doxorubicin (DOX), navelbine (NVB), cisplatin, 3-(4, 5-dimethylthiazol-2-yl)-2, 5-diphenyltetrazolium bromide (MTT), and dimethyl sulfoxide (DMSO) were all purchased from Sigma-Aldrich (St. Louis, MO, USA).

### 3.5. Cell Cytotoxicity Assay

Cell cytotoxicity assay *in vitro* was evaluated by MTT assay, as described previously [36]. In brief, cells were seeded in 96-well plates at an appropriate density and incubated for 24 h at 37 °C. Then, the cells were treated with various concentrations of chemotherapeutic drugs or compounds. A total of 20 µL of MTT solution (5 mg/mL in PBS) was added to each well after 72 h incubation. The plates were incubated at 37 °C for another 4 h and the resulting formazan crystals were dissolved with 150 µL DMSO. Absorbance in each well was measured by Model 550 Microplate Reader (Bio-Rad, Hercules, CA, USA) at 570 nm. The half maximal (50%) inhibitory concentration (IC<sub>50</sub>) was calculated from the curves using GraphPad Prism 9.0, using the Bliss method [37]. The maximal concentration of compound **8** indicated that a cell survival of more than 80% was required when testing its MDR-reversal effect. The effect of the MDR reversal by compound **8** was calculated by dividing the IC<sub>50</sub> of cells treated with chemotherapeutic drugs alone or by the IC<sub>50</sub> of cells treated with chemotherapeutic drugs in the presence of compound **8**. All experiments were repeated at least three times.

### 3.6. DOX Accumulation Assay

A flow cytometry assay was performed to examine whether compounds **1–10** could affect the accumulation of DOX in KBv200 or HeLa/VCR cells, as previously described [36]. In brief, the logarithmically growing KBv200 or HeLa/VCR cells were seeded in six-well plates at a density of 3 × 10<sup>5</sup> per well. After 24 h of incubation, the cells were pretreated with 20 µM of compounds **1–10** or various concentrations of compound **8** or the vehicle for 3 h at 37 °C. Then, cells were further incubated with 10 µM DOX for another 3 h. After that, the cells were collected, washed three times with cold phosphate-buffered saline (PBS), and resuspended in 500 µL PBS. The mean fluorescence intensity (MFI) of DOX was examined via flow cytometry (Cytomics FC500, Beckman Coulter Inc., Brea, CA, USA) with an excitation wavelength of 488 nm and an emission wavelength of 550 nm.

### 3.7. Molecular Docking Analysis

The crystal structures of the ABCB1 protein [38] (PDB ID: 6QEX) used for docking were downloaded from the PDB database. The 3D structure of the small molecule complex was constructed using Chem3D 20.0 and energy was minimized under the MMFF94 force field. Before ligand docking, PyMol 2.5.5 [39] was used to treat the receptor protein, including the removal of water molecules, salt ions, and small molecules. Subsequently, a 25 × 25 × 25 grid box, with the center being the center of the crystal ligand, was set up. In addition, ADFRsuite 1.0 [40] was used to convert all processed small molecules and receptor proteins into the necessary PDBQT format for AutoDock Vina 1.1.2 [41] docking software. When docking, the global search granularity was set to 32, while the remaining parameters remained at their default settings. The top-scoring model (based on the docking score in kcal/mol) was visualized and analyzed using PyMol 2.5.5.

### 3.8. Data Analysis

All data are expressed as mean  $\pm$  standard deviation (mean  $\pm$  SD) established in different experiments and analyzed by one-way analysis of variance (ANOVA), followed by Bonferroni post hoc test. Statistical graphs were produced by GraphPad Prism 9.0.0 software (GraphPad Software, Inc., San Diego, CA, USA). \*,  $p < 0.05$ ; \*\*,  $p < 0.01$ ; \*\*\*,  $p < 0.001$ , was considered statistically significant.

## 4. Conclusions

In this study, two new phenylspirodrimanones, stachybotrin K (1), and stachybotrin L (2), together with eight known derivatives (3–10), were isolated from deep-sea-derived *Stachybotrys* sp. MCCC 3A00409. Extensive NMR spectroscopic analysis and ECD analysis were used to elucidate the structures of new compounds, including their absolute configurations. The screening results of all compounds with resistance reversal activity in a drug-resistant tumor cell line showed that stachybotrysin B (8) had the most significant effect. Compound 8 exhibited resistance reversal effects against the substrate chemotherapeutic agents, doxorubicin (DOX), and navelbine (NVB) in the ABCB1-overexpressing drug-resistant cell line KBv200, and against DOX in the ABCB1-overexpressing drug-resistant cell line Hela/VCR, in a dose-dependent manner. The results of flow cytometry analysis showed that the mechanism of its MDR reversal effect might be related to the increase in the intracellular concentration of substrate anticancer drug. The docking analysis of compound 8 binding to ABCB1 transporter protein indicated that 8 can potentially strongly interact with several amino acid residues within the transmembrane regions of ABCB1. This interaction might inhibit the efflux of substrates such as DOX, thereby increasing the accumulation of DOX in ABCB1-resistant cancer cells and reversing ABCB1-mediated multidrug resistance.

**Supplementary Materials:** The following supporting information can be downloaded at: <https://www.mdpi.com/article/10.3390/molecules29071685/s1>, Figure S1: Key  $^1\text{H}$ - $^1\text{H}$  COSY, HMBC, and NOESY correlations of 2; Figure S2:  $^1\text{H}$  NMR spectrum (400 MHz) of stachybotrin K (1) in DMSO- $d_6$ ; Figure S3:  $^{13}\text{C}$  NMR spectrum (100 MHz) of stachybotrin K (1) in DMSO- $d_6$ ; Figure S4:  $^1\text{H}$  NMR spectrum (600 MHz) of stachybotrin K (1) in DMSO- $d_6$ ; Figure S5:  $^{13}\text{C}$  NMR spectrum (150 MHz) of stachybotrin K (1) in DMSO- $d_6$ ; Figure S6: DEPT 90 spectrum (100 MHz) of stachybotrin K (1) in DMSO- $d_6$ ; Figure S7: DEPT 135 spectrum (100 MHz) of stachybotrin K (1) in DMSO- $d_6$ ; Figure S8: HMQC spectrum of stachybotrin K (1) in DMSO- $d_6$ ; Figure S9:  $^1\text{H}$ - $^1\text{H}$  COSY spectrum of stachybotrin K (1) in DMSO- $d_6$ ; Figure S10: HMBC spectrum of stachybotrin K (1) in DMSO- $d_6$ ; Figure S11: ROSEY spectrum of stachybotrin K (1) in DMSO- $d_6$ ; Figure S12: HRESIMS spectrum of stachybotrin K (1); Figure S13:  $^1\text{H}$  NMR spectrum (400 MHz) of stachybotrin L (2) in DMSO- $d_6$ ; Figure S14:  $^{13}\text{C}$  NMR spectrum (100 MHz) of stachybotrin L (2) in DMSO- $d_6$ ; Figure S15:  $^1\text{H}$  NMR spectrum (600 MHz) of stachybotrin L (2) in DMSO- $d_6$ ; Figure S16:  $^{13}\text{C}$  NMR spectrum (150 MHz) of stachybotrin L (2) in DMSO- $d_6$ ; Figure S17: DEPT 90 spectrum (100 MHz) of stachybotrin K (2) in DMSO- $d_6$ ; Figure S18: DEPT 135 spectrum (100 MHz) of stachybotrin K (2) in DMSO- $d_6$ ; Figure S19: HMQC spectrum of stachybotrin L (2) in DMSO- $d_6$ ; Figure S20:  $^1\text{H}$ - $^1\text{H}$  COSY spectrum of stachybotrin L (2) in DMSO- $d_6$ ; Figure S21: HMBC spectrum of stachybotrin L (2) in DMSO- $d_6$ ; Figure S22: ROSEY spectrum of stachybotrin L (2) in DMSO- $d_6$ ; Figure S23: HRESIMS spectrum of stachybotrin L (2).

**Author Contributions:** Conceptualization, Z.Z. and L.C.; methodology, M.W., Z.C. and F.C.; formal analysis, T.Z.; resources, Z.L. and Z.S.; writing—original draft preparation, X.M.; writing—review and editing, Z.Z.; visualization, X.M.; supervision, Y.Z. All authors have read and agreed to the published version of the manuscript.

**Funding:** The study was supported by Natural Science Foundation of Fujian Province (No. 2018J01847, 2023J01550), and the National Natural Science Foundation of China (No. 41806173), Open Research Fund of Fujian Key Laboratory of Natural Medicine Pharmacology (No. FJNMP-202203).

**Data Availability Statement:** Data are contained within the article and Supplementary Materials.

**Acknowledgments:** We are grateful to Marine Culture Collection Center (MCCC), Third Institute of Oceanography, Ministry of Natural Sources for providing the strain.

**Conflicts of Interest:** The authors declare no conflicts of interest.

## References

1. Sameiyan, E.; Hayes, A.W.; Karimi, G. The effect of medicinal plants on multiple drug resistance through autophagy: A review of in vitro studies. *Eur. J. Pharmacol.* **2019**, *852*, 244–253.
2. Luqmani, Y.A. Mechanisms of drug resistance in cancer chemotherapy. *Med. Princ. Pract.* **2005**, *14*, 35–48.
3. Zhang, Z.; Ma, C.; Li, P.; Wu, M.; Ye, S.; Fu, L.; Xu, J. Reversal effect of FW-04-806, a macrolide dilactone compound, on multi-drug resistance mediated by ABCB1 and ABCG2 in vitro and in vivo. *Cell Commun. Signal.* **2019**, *17*, 110.
4. Szakács, G.; Paterson, J.K.; Ludwig, J.A.; Booth-Genthe, C.; Gottesman, M.M. Targeting multidrug resistance in cancer. *Nat. Rev. Drug Discov.* **2006**, *5*, 219–234.
5. Kumar, A.; Jaitak, V. Natural products as multidrug resistance modulators in cancer. *Eur. J. Med. Chem.* **2019**, *176*, 268–291.
6. Kartal-Yandim, M.; Adan-Gokbulut, A.; Baran, Y. Molecular mechanisms of drug resistance and its reversal in cancer. *Crit. Rev. Biotechnol.* **2016**, *36*, 716–726.
7. Gameiro, M.; Silva, R.; Rocha-Pereira, C.; Carmo, H.; Carvalho, F.; Bastos, M.L.; Remião, F. Cellular models and in vitro assays for the screening of modulators of P-gp, MRP1 and BCRP. *Molecules* **2017**, *22*, 600.
8. Engle, K.; Kumar, G. Cancer multidrug-resistance reversal by ABCB1 inhibition: A recent update. *Eur. J. Med. Chem.* **2022**, *239*, 114542.
9. Lai, J.L.; Tseng, Y.J.; Chen, M.H.; Huang, C.F.; Chang, P.M. Clinical perspective of FDA approved drugs with P-glycoprotein inhibition activities for potential cancer therapeutics. *Front. Oncol.* **2020**, *10*, 561936.
10. Chen, Z.; Chen, Y.; Xu, M.; Chen, L.; Zhang, X.; To, K.K.; Zhao, H.; Wang, F.; Xia, Z.; Chen, X.; et al. Osimertinib (AZD9291) enhanced the efficacy of chemotherapeutic agents in ABCB1- and ABCG2-overexpressing cells in vitro, in vivo, and ex vivo. *Mol. Cancer Ther.* **2016**, *15*, 1845–1858.
11. Yang, K.; Chen, Y.; To, K.K.; Wang, F.; Li, D.; Chen, L.; Fu, L. Alectinib (CH5424802) antagonizes ABCB1- and ABCG2-mediated multidrug resistance in vitro, in vivo and ex vivo. *Exp. Mol. Med.* **2017**, *49*, e303.
12. Karthikeyan, S.; Hoti, S.L. Development of fourth generation ABC inhibitors from natural products: A novel approach to overcome cancer multidrug resistance. *Anticancer Agents Med. Chem.* **2015**, *15*, 605–615.
13. Yang, Z.; Yang, X.; Li, Y.; Cai, Y.; Yu, Y.; Zhuang, W.; Sun, X.; Li, Q.; Bao, X.; Ye, X.; et al. Design, synthesis and biological evaluation of novel phenylfuran-bisamide derivatives as P-glycoprotein inhibitors against multidrug resistance in MCF-7/ADR cell. *Eur. J. Med. Chem.* **2023**, *248*, 115092.
14. Ross, D.D. Modulation of drug resistance transporters as a strategy for treating myelodysplastic syndrome. *Best Pract. Res. Clin. Haematol.* **2004**, *17*, 641–651.
15. Gandhi, L.; Harding, M.W.; Neubauer, M.; Langer, C.J.; Moore, M.; Ross, H.J.; Johnson, B.E.; Lynch, T.J. A phase II study of the safety and efficacy of the multidrug resistance inhibitor VX-710 combined with doxorubicin and vincristine in patients with recurrent small cell lung cancer. *Cancer* **2007**, *109*, 924–932.
16. Chi, K.N.; Chia, S.K.; Dixon, R.; Newman, M.J.; Wacher, V.J.; Sikic, B.; Gelmon, K.A. A phase I pharmacokinetic study of the P-glycoprotein inhibitor, ONT-093, in combination with paclitaxel in patients with advanced cancer. *Investig. New Drugs.* **2005**, *23*, 311–315.
17. Ma, Y.; Yin, D.; Ye, J.; Wei, X.; Pei, Y.; Li, X.; Si, G.; Chen, X.Y.; Chen, Z.S.; Dong, Y.; et al. Discovery of potent inhibitors against P-glycoprotein-mediated multidrug resistance aided by late-stage functionalization of a 2-(4-(pyridin-2-yl)phenoxy)pyridine analogue. *J. Med. Chem.* **2020**, *63*, 5458–5476.
18. Waghay, D.; Zhang, Q. Inhibit or evade multidrug resistance P-glycoprotein in cancer treatment. *J. Med. Chem.* **2018**, *61*, 5108–5121.
19. Ibrahim, S.R.M.; Choudhry, H.; Asseri, A.H.; Elfaky, M.A.; Mohamed, S.G.A.; Mohamed, G.A. *Stachybotrys chartarum*-A hidden treasure: Secondary metabolites, bioactivities, and biotechnological relevance. *J. Fungi* **2022**, *8*, 504.
20. Wang, A.; Xu, Y.; Gao, Y.; Huang, Q.; Luo, X.; An, H.; Dong, J. Chemical and bioactive diversities of the genera *Stachybotrys*. *Phytochem. Rev.* **2015**, *14*, 623–655.
21. Wang, S.; Li, S.; Chen, Y.; Wang, Y.; Liu, Z.; Zhang, W.; Deng, H. A new phenylspirodrimane derivative from the deep-sea-derived fungus *Stachybotrys chartarum* FS705. *Nat. Prod. Res.* **2024**, *22*, 1–7.
22. Dayras, M.; Sfecci, E.; Bovio, E.; Rastoin, O.; Dufies, M.; Fontaine-Vive, F.; Taffin-de-Givenchy, E.; Lacour, T.; Pages, G.; Varese, G.C.; et al. New phenylspirodrimanes from the sponge-associated fungus *Stachybotrys chartarum* MUT 3308. *Mar. Drugs* **2023**, *21*, 135.
23. Bao, Y.R.; Feng, H.L.; Yao, X.S. *Stachybotranes A-D*, phenylspirodrimanes from the wetland fungus *Stachybotrys chartarum* with cytotoxic activities. *Nat. Prod. Res.* **2022**, *36*, 3894–3900.
24. Jagels, A.; Hövelmann, Y.; Zielinski, A.; Esselen, M.; Köhler, J.; Hübner, F.; Humpf, H. *Stachybotrychromenes A-C*: Novel cytotoxic meroterpenoids from *Stachybotrys* sp. *Mycotoxin Res.* **2018**, *534*, 179–185.
25. Ma, X.; Li, L.; Zhu, T.; Ba, M.; Li, G.; Gu, Q.; Guo, Y.; Li, D. Phenylspirodrimanes with anti-HIV activity from the sponge-derived fungus *Stachybotrys chartarum* MXH-X73. *J. Nat. Prod.* **2013**, *76*, 2298–2306.

26. Ma, X.H.; Zheng, W.M.; Sun, K.H.; Gu, X.F.; Zeng, X.M.; Zhang, H.T.; Zhong, T.H.; Shao, Z.Z.; Zhang, Y.H. Two new phenylspirodrimanes from the deep-sea derived fungus *Stachybotrys* sp. MCCC 3A00409. *Nat. Prod. Res.* **2019**, *33*, 386–392.
27. Zhang, P.P.; Li, Y.F.; Jia, C.X.; Lang, J.J.; Niaz, S.I.; Li, J. Antiviral and anti-inflammatory meroterpenoids: Stachybonoids A-F from the crinoid-derived fungus *Stachybotrys chartarum* 952. *RSC Adv.* **2017**, *7*, 49910–49916.
28. Feng, J.M.; Li, M.; Zhao, J.L.; Jia, X.N.; Liu, J.M.; Zhang, M.; Chen, R.D.; Xie, K.B.; Chen, D.W.; Yu, H.B.; et al. Three new phenylspirodrimane derivatives with inhibitory effect towards potassium channel Kv1.3 from the fungus *Stachybotrys chartarum*. *J. Asian Nat. Prod. Res.* **2019**, *21*, 887–894.
29. Jarvis, B.B.; Salemme, J.; Morais, A. Stachybotrys toxins. 1. *Nat. Toxins* **1995**, *3*, 10–16.
30. Zhao, J.; Feng, J.; Tan, Z.; Liu, J.; Zhao, J.; Chen, R.; Xie, K.; Zhang, D.; Li, Y.; Yu, L.; et al. Stachybotrysins A-G, phenylspirodrimane derivatives from the fungus *Stachybotrys chartarum*. *J. Nat. Prod.* **2017**, *80*, 1819–1826.
31. Kaneto, R.; Dobashi, K.; Kojima, I.; Sakai, K.; Shibamoto, N.; Yoshika, T.; Nishida, H.; Okamoto, R.; Akagawa, H.; Mizuno, S.; et al. Mer-NF5003B, E and F, novel sesquiterpenoids as avian myeloblastosis virus protease inhibitors produced by *Stachybotrys* sp. *J. Antibiot.* **1994**, *47*, 727–730.
32. Liang, B.J.; Lusvardi, S.; Ambudkar, S.V.; Huang, H.C. Mechanistic insights into photodynamic regulation of adenosine 5'-triphosphate-binding cassette drug transporters. *ACS Pharmacol. Transl. Sci.* **2021**, *4*, 1578–1587.
33. Wu, C.P.; Hsiao, S.H.; Huang, Y.H.; Hung, L.C.; Yu, Y.J.; Chang, Y.T.; Hung, T.H.; Wu, Y.S. Sitravatinib sensitizes ABCB1- and ABCG2-overexpressing multidrug-resistant cancer cells to chemotherapeutic drugs. *Cancers* **2020**, *12*, 195.
34. Narayanan, S.; Gujarati, N.A.; Wang, J.Q.; Wu, Z.X.; Koya, J.; Cui, Q.; Korlipara, V.L.; Ashby, C.R., Jr.; Chen, Z.S. The novel benzamide derivative, VKNG-2, restores the efficacy of chemotherapeutic drugs in colon cancer cell lines by inhibiting the ABCG2 transporter. *Int. J. Mol. Sci.* **2021**, *22*, 2463.
35. Wang, X.; Zhang, T.; Chen, X.; Xu, Y.; Li, Z.; Yang, Y.; Du, X.; Jiang, Z.; Ni, H. Simultaneous inhibitory effects of all-trans astaxanthin on acetylcholinesterase and oxidative stress. *Mar. Drugs* **2022**, *20*, 247.
36. Wu, M.; Shen, C.E.; Lin, Q.F.; Zhong, J.Y.; Zhou, Y.F.; Liu, B.C.; Xu, J.H.; Zhang, Z.Q.; Li, P. Sterols and triterpenoids from *Ganoderma lucidum* and their reversal activities of tumor multidrug resistance. *Nat. Prod. Res.* **2022**, *36*, 1396–1399.
37. Shi, Z.; Liang, Y.J.; Chen, Z.S.; Wang, X.W.; Wang, X.H.; Ding, Y.; Chen, L.M.; Yang, X.P.; Fu, L.W. Reversal of MDR1/P-glycoprotein-mediated multidrug resistance by vector-based RNA interference in vitro and in vivo. *Cancer Biol. Ther.* **2006**, *5*, 39–47.
38. Alam, A.; Kowal, J.; Broude, E.; Roninson, I.; Locher, K.P. Structural insight into substrate and inhibitor discrimination by human P-glycoprotein. *Science* **2019**, *363*, 753–756.
39. DeLano, W.L. Pymol: An open-source molecular graphics tool. *CCP4 Newsl. Protein Crystallogr.* **2002**, *40*, 82–92.
40. Ravindranath, P.A.; Forli, S.; Goodsell, D.S.; Olson, A.J.; Sanner, M.F. AutoDockFR: Advances in protein-ligand docking with explicitly specified binding site flexibility. *PLoS Comput. Biol.* **2015**, *11*, e1004586.
41. Trott, O.; Olson, A.J. AutoDock Vina: Improving the speed and accuracy of docking with a new scoring function, efficient optimization, and multithreading. *J. Comput. Chem.* **2010**, *31*, 455–461.

**Disclaimer/Publisher's Note:** The statements, opinions and data contained in all publications are solely those of the individual author(s) and contributor(s) and not of MDPI and/or the editor(s). MDPI and/or the editor(s) disclaim responsibility for any injury to people or property resulting from any ideas, methods, instructions or products referred to in the content.